Decentralized Passivity-Based Control With a Generalized Energy Storage Function for Robust Biped Locomotion

Mark Yeatman
Department of Mechanical Engineering,
University of Texas at Dallas,
Richardson, TX 75080

Ge Lv
Department of Electrical Engineering,
University of Texas at Dallas,
Richardson, TX 75080

Robert D. Gregg[1]
Department of Bioengineering;
Department of Mechanical Engineering,
University of Texas at Dallas,
Richardson, TX 75080
e-mail: rgregg@ieee.org

This paper details a decentralized passivity-based control (PBC) to improve the robustness of biped locomotion in the presence of gait-generating external torques and parametric errors in the biped model. Previous work demonstrated a passive output for biped systems based on a generalized energy that, when directly used for feedback control, increases the basin of attraction and convergence rate of the biped to a stable limit cycle. This paper extends the concept with a theoretical framework to address both uncertainty in the biped model and a lack of sensing hardware, by allowing the designer to neglect arbitrary states and parameters in the system. This framework also allows the control to be implemented on wearable devices, such as a lower limb exoskeleton or powered prosthesis, without needing a model of the user's dynamics. Simulations on a six-link biped model demonstrate that the proposed control scheme increases the convergence rate of the biped to a walking gait and improves the robustness to perturbations and to changes in ground slope. [DOI: 10.1115/1.4043801]

1 Introduction

Autonomous biped control is an application defined by a number of challenges including nonlinear dynamics, hybrid dynamics, and underactuation. One of the classic goals of control design for these systems is to drive the joint torques of the biped to perform some repetitive locomotion task, like walking or running, which can be modeled with a nonlinear stability concept called a limit cycle (i.e., a periodic orbit in the state space of the system) [1]. This limit cycle experiences discrete jumps in velocity due to hybrid dynamics that model the plastic impacts of the biped with the ground. Underactuation restricts the ability to arbitrarily control the dynamics of the biped to generate a desired limit cycle [2]. It is possible to embrace this property and design controllers, which stabilize desired trajectories based on hybrid zero dynamics, as in Ref. [3]. This methodology has been implemented on a wide range of systems, as demonstrated in Refs. [4] and [5]. However, these trajectories are designed for specific tasks and with specific optimization criteria. Trajectory-free control methods are of interest for a more task-invariant approach.

A particularly well-known phenomenon in biped locomotion is that of passive dynamic walking, as first reported by McGeer [6], where an uncontrolled biped is able to walk down a shallow slope under the power of gravity. In other words, a stable limit cycle can naturally emerge from the interaction of the biped with the environment. The basin of attraction of the natural limit cycle is quite small, meaning that it will only converge to the walking gait from a small set of states. The limit cycle can be characterized by the equilibrium between the simultaneous decrease of kinetic energy and increase of potential energy at impact, which causes the mechanical energy of the system to be conserved along the limit cycle. Goswami et al. were the first to exploit these natural dynamics and use passivity-based control (PBC) to drive the biped's energy to this conserved value, in order to enlarge the basin of attraction of the limit cycle in a trajectory free manner [1]. A PBC is a control law that exploits an input–output relationship that bounds the rate of change of an energy-like storage function in the system, and is complimentary related to the idea of passive walking.

Others have built on these ideas and demonstrated more sophisticated examples of energy-based control for biped locomotion [7]. Methodologies such as energy shaping [8–12], interconnection and damping assignment-PBC [13], and the rapidly exponentially stabilizing control Lyapunov function [14] have also utilized these connections between energy and limit cycles to create stable walking gaits. However, these methods have their limitations. Energy shaping and interconnection and damping assignment-PBC rely on the system meeting a matching criterion that restricts the degree of underactuation allowed and generally requires an inversion of the system mass matrix, which can be sensitive to error in the model parameters. The energy tracking PBC methods in Refs. [1] and [7] require a conserved mechanical energy, which is impractical for a real system. The rapidly exponentially stabilizing control Lyapunov function method [15] does not have a demonstrated passivity property to date, which can limit its performance in uncertain environments (i.e., unknown terrains or human–robot interactions). Recently, concepts from Ref. [15] were leveraged to generalize the energy tracking method of Ref. [7] to bipeds with pre-existing control inputs that do work (e.g., human locomotion), while also allowing arbitrary underactuation in the PBC [16]. However, this control approach required full knowledge of the state variables and model parameters, which presents significant implementation challenges.

This paper addresses this gap by developing a new decentralized formulation that provides a theoretical framework to address both uncertainty in the biped model and a lack of sensing, by allowing the designer to ignore arbitrary states and model parameters in the system. A decentralized control scheme, in general, utilizes multiple subcontrollers working in concert to achieve a task [17]. Each controller only has access to a subset of the state and model information (termed "local" information). This scheme is desirable in the control of biped locomotion for a number of reasons. It can allow for a reduction of sensing components in the

[1]Corresponding author.

Contributed by the Dynamic Systems Division of ASME for publication in the Journal of Dynamic Systems, Measurement, and Control. Manuscript received September 9, 2018; final manuscript received May 14, 2019; published online June 13, 2019. Assoc. Editor: Inna Sharf.

hardware, compensate for uncertainties in the dynamic model of the biped, and reduce the computational complexity of the control [18,19]. It is of critical concern when considering the potential application to wearable devices (e.g., a powered prosthesis or lower limb exoskeleton) where a user guides and generates their own limit cycle, but a high fidelity model for their dynamics cannot be obtained [20]. The decentralized PBC retains useful qualities of the centralized approach, such as arbitrary underactuation, synergy with inner loop controllers, and improved robustness and convergence rate of the limit cycle.

The format of the paper is as follows: Sec. 2 introduces the hybrid dynamic model of a six-link biped and a proportional-derivative (PD) controller that generates a walking gait for the biped. Section 3 offers a brief review of passivity and derives a centralized PBC from an energy-based storage function. Numerical simulations of this control applied to the biped model are given. Section 4 extends the PBC with a decentralized formulation that bases the construction of the storage function on a Lagrangian subsystem; then comparisons between the simulations of the centralized and decentralized PBCs are made. Section 5 offers a modification of the PBCs that has an adaptive reference energy. Section 6 discusses issues of implementation on a physical system and offers a potential method of achieving this. Section 7 contains concluding remarks and ideas for future work.

Notation: Given two matrices a and b of suitable dimensions, the matrix $[a^\top, b^\top]^\top$ where $\top$ denotes the transpose operator is denoted by $[a; b]$.

2 Modeling and Dynamics

In this paper, we use the model given in Ref. [21] and offer a brief review of it in this section. For simplicity, the link between the two hip joints is modeled as a single joint and there is no torso link. Thus, together with a foot, shank, and thigh link for each leg, the model is a six-link biped. The biped is modeled as a planar kinematic chain with respect to an inertial reference frame defined at either the stance heel or stance toe, depending on the phase of the single-support period (to be discussed in Sec. 2.2). A diagram of the biped is shown in Fig. 1.

The generalized coordinates of the biped model are defined as $q = [p_x, p_y, \phi, \theta_a, \theta_k, \theta_h, \theta_{sk}, \theta_{sa}]^\top \in \mathbb{R}^{8\times 1}$, where p_x and p_y represent the Cartesian position of the stance heel or stance toe in the inertial reference frame, and ϕ is the angle of the heel-to-ankle vector with respect to the vertical axis. The subscript $i \in \{a, k, h, sk, sa\}$ denotes the ankle, knee, hip, stance knee, and stance ankle, respectively, and is used to describe the angles θ_i between each link. The mass m_j, length l_j, and inertia I_j of the links are indexed by the subscript $j \in \{f, s, t, h, st, ss, sf\}$, which denotes the stance foot, stance shank, stance thigh, hip, swing thigh, swing shank, and swing foot, respectively.

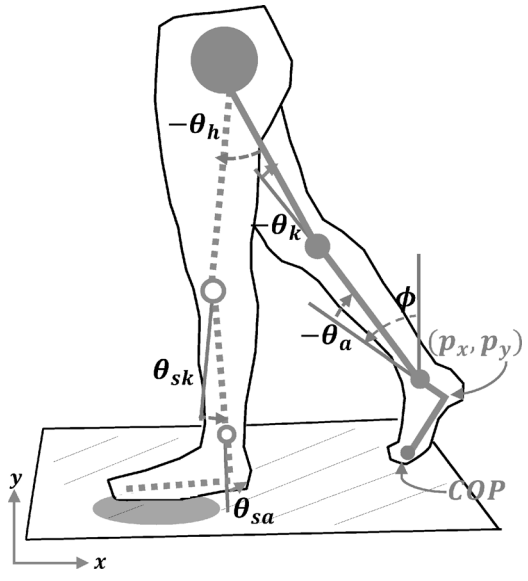

Fig. 1 Kinematic model of the biped. COP denotes the center of pressure. The solid links denote the stance leg and the dashed links denote the swing leg.

2.1 Continuous Lagrangian Dynamics.

The dynamics are derived using the Lagrangian formulation [22] to obtain the equation

$$M(q)\ddot{q} + C(q,\dot{q})\dot{q} + N(q) + A(q)^\top \lambda = \tau \tag{1}$$

where $M(q) \in \mathbb{R}^{8\times 8}$ is the inertia matrix, $C(q,\dot{q}) \in \mathbb{R}^{8\times 8}$ is the Coriolis/centrifugal matrix, and $N(q) \in \mathbb{R}^{8\times 1}$ is the gravity force vector. The term $A(q)^\top \lambda$ models the interaction between the biped's foot and the ground, where the matrix $A(q) \in \mathbb{R}^{c\times 8}$ is defined as the gradient of the constraint functions, and c is the number of contact constraints that may change during different contact conditions. The Lagrange multiplier $\lambda \in \mathbb{R}^{c\times 1}$ is calculated using the method in Refs. [21] and [23] and satisfies the assumption that the ground reaction forces do no work on the system. The torque vector is $\tau = B_u u + B_v v$, where $B_u \in \mathbb{R}^{8\times d}$ and $B_v \in \mathbb{R}^{8\times m}$ map the PBC torques u and additional control torques v (to be defined in Sec. 2.4) into the generalized coordinates, respectively. The number of control inputs d and m do not need to be the same.

2.2 Contact Constraints.

Based on Refs. [24] and [25], the single-support period can be broken down into three subphases: heel contact, flat foot, and toe contact, where holonomic contact constraints can be properly defined. Following the convention in Ref. [21], we express the holonomic contact constraints of the biped as relations between the position variables of the form

$$a_{\text{sub}}(q_1, q_2, \ldots, q_c) = 0_{c\times 1} \tag{2}$$

where q_j denotes the jth element of the configuration vector q and $\text{sub} \in \{\text{heel}, \text{flat}, \text{toe}\}$ indicates the contact phase. There are $c = 2$ constraints for heel contact and toe contact, whereas flat foot has $c = 3$ constraints. The constraint matrix can then be defined for all contact conditions as

$$A_{\text{sub}} = \frac{\partial a(q)}{\partial q} = \begin{bmatrix} I_{c\times c} & 0_{c\times(8-c)} \end{bmatrix} \tag{3}$$

This form can be achieved by defining the inertial reference frame at the stance heel during heel contact and flat foot, and at the stance toe during toe contact.

2.3 Hybrid Dynamics.

Biped locomotion can be modeled as a hybrid dynamical system, which includes continuous and discrete dynamics [26]. The system follows a sequence of continuous dynamics and their discrete transitions. It cycles through different contact configurations defined in Sec. 2.2 during stance period and encounters impacts when the swing heel hits the ground or the flat foot slaps the ground. Following the same assumption in Ref. [26], the discrete transitions model an instantaneous double-support phase at heel strike and plastic impacts. The map from pre-impact state to postimpact state is derived based on the assumption that the impact impulsively constrains the contact point to the ground, which can cause an instant change in the velocity and thus the kinetic energy of the biped.

Based on the method in Ref. [21], the hybrid dynamic regimes over one step are computed in the following sequence:

Heel regime

$$\begin{aligned}
&(1)\ \ M\ddot{q} + T(q,\dot{q}) + A_{\text{heel}}^{\top}\lambda = \tau && \text{if} \quad a_{\text{flat}} \neq 0\\
&(2)\ \ \dot{q}^{+} = (I - X(A_{\text{flat}}X)^{-1}A_{\text{flat}})\dot{q}^{-} && \text{if} \quad a_{\text{flat}} = 0
\end{aligned}$$

Flat regime

$$\begin{aligned}
&(3)\ \ M\ddot{q} + T(q,\dot{q}) + A_{\text{flat}}^{\top}\lambda = \tau && \text{if} \quad |c_{\text{p}}(q,\dot{q})| < l_{\text{f}}\\
&(4)\ \ \dot{q}^{+} = \dot{q}^{-}, (q(1)^{+}, q(2)^{+})^{\top} = \mathcal{G} && \text{if} \quad |c_{\text{p}}(q,\dot{q})| = l_{\text{f}}
\end{aligned}$$

Toe regime

$$\begin{aligned}
&(5)\ \ M\ddot{q} + T(q,\dot{q}) + A_{\text{toe}}^{\top}\lambda = \tau && \text{if} \quad h(q) \neq 0\\
&(6)\ \ (q^{+},\dot{q}^{+}) = R(q^{-},\dot{q}^{-}) && \text{if} \quad h(q) = 0
\end{aligned}$$

The vector T groups the Coriolis/centrifugal terms and potential forces for brevity. The superscripts "–" and "+" indicate the pre-impact and the postimpact values, respectively. The terms $X = M^{-1}A_{\text{flat}}^{\top}$ and $\mathcal{G} = (l_{\text{f}}\cos(\gamma), l_{\text{f}}\sin(\gamma))^{\top}$ model the change in inertial reference frame, c_p is the location of the center of pressure, γ is the ground slope angle, and l_f is the foot length. The ground clearance of the swing heel is denoted by $h(q)$, and R denotes the swing heel ground-strike impact map derived based on Ref. [26].

2.4 Inner Loop Proportional-Derivative Control. Part of the model from Ref. [21] is a set-point PD controller that generates a stable limit cycle while walking down a shallow slope. It has the form

$$v = -K_p(q_m - \bar{\theta}) - K_d\,\dot{q}_m \tag{4}$$

Here, q_m is the actuated coordinates vector, $\bar{\theta}$ is the equilibrium vector, and the diagonal control gain matrices are denoted as $K_p, K_d \in \mathbb{R}^{5\times5}$. The mapping matrix B_v is constructed such that the PD controller actuates the ankles, knees, and hip of the biped. We term this PD controller v the "inner loop" and the to-be-derived PBC u the "outer loop," since the PBC derivation relies on the existence a limit cycle.

3 Centralized Passivity-Based Control

The passive compass-gait biped has no external force input during its continuous dynamics; thus, the only work done on the system is by the discrete impacts with the ground. On a passive limit cycle, the kinetic energy of the biped is essentially reset after each impact, while the datum defining the potential energy is shifted to reset the potential energy. This gives rise to a constant system energy [1]. A similar phenomenon exists for an n-link biped on a limit cycle generated by a controller v that does work. During the continuous dynamics, the work done by the controller exactly accounts for the change in the mechanical energy. If the work is reset to zero after each impact (which we can enforce by convention), this gives rise to a sequence of generalized system energies that are conserved on the limit cycle [15]. We seek to utilize this conservation to formulate a passivity-based control u that increases the basin of attraction of the pre-existing limit cycle.

The concept of passivity is a powerful tool for analyzing the stability of nonlinear systems and designing controllers for those systems, and it is distinct from the way "passive" is used to describe the compass gait walker. Passive in that context means there is no actuation, while passivity is an input–output relationship of dynamic systems. Historically, it has been used to show that the change of energy in a system is bounded by a function of the control input and establish stability proofs using arguments similar to the method of Lyapunov [22]. The formal definition for passivity is given as follows [27]:

DEFINITION 1. *Let $S(q,\dot{q}) : \mathbb{R}^{2n} \to \mathbb{R}$ be a continuously differentiable, non-negative scalar function. A system is passive from input u to output y with storage function $S(q,\dot{q})$ if $\dot{S}(q,\dot{q}) \leq y^{\top}u$.*

The mechanical energy of a system often acts as the storage function and the output is the vector of joint velocities [28]. However, a storage function does not have to be a quantity with a direct physical interpretation. We use an energy-squared storage function, which can be interpreted as the distance between a given state vector and the desired energy state. The main idea behind the control is to feedback the passive output as $u = -y$ to drive this distance to zero, and thus drive the system to the limit cycle. In the analysis, the arguments of dependent variables or functions will sometimes be dropped for conciseness.

3.1 Centralized Derivation. As shown in Ref. [15], we can define a generalized system energy as

$$E(q,\dot{q},v,t) = K(q,\dot{q}) + P(q) - W(q,\dot{q},v,t) \tag{5}$$

The mechanical energy of the system is the kinetic energy K plus the potential energy P, while the work done by the inner loop controller is

$$W = \int_0^t \dot{q}^{\top}B_v v\,d\tau \tag{6}$$

The work W accounts for the energy stored, added, and dissipated over time t by the inner loop control torque v. Note that the exact form of this control is left arbitrary. In the following analysis, the important feature is that it generates a limit cycle for the biped.

Consider the following storage function from Ref. [29] for the derivation of a passivity-based controller:

$$S(q,\dot{q}) = \frac{1}{2}(E - E_{\text{ref}})^2 \tag{7}$$

where E_{ref} is the constant reference energy defined on a given limit cycle. Taking the time-derivative of S, we obtain

$$\dot{S} = (E - E_{\text{ref}})(\dot{E} - \dot{E}_{\text{ref}}) \tag{8}$$

Since E_{ref} is constant, $\dot{E}_{\text{ref}} = 0$ and all that remains is to calculate $\dot{E}$. From Eqs. (5) and (1), the time-derivative is

$$\dot{E} = \frac{d(K+P)}{dt} - \frac{dW}{dt} \tag{9}$$

From the definition of W, the application of the fundamental theorem of calculus, and the conservation of energy in a mechanical system

$$\dot{E} = (\dot{q}^{\top}B_u u + \dot{q}^{\top}B_v v) - \dot{q}^{\top}B_v v = \dot{q}^{\top}B_u u \tag{10}$$

It follows that the time-derivative of the storage function becomes:

$$\dot{S} = (E - E_{\text{ref}})\dot{q}^{\top}B_u u \tag{11}$$

with passive output

$$y(q,\dot{q},v,t)^{\top} = (E - E_{\text{ref}})\dot{q}^{\top}B_u \in \mathbb{R}^{1\times d} \tag{12}$$

Following the paradigm of passive output feedback, the PBC is:

$$u(q,\dot{q},v,t) = -k\Omega y = -k\Omega(E - E_{\text{ref}})B_u^{\top}\dot{q} \tag{13}$$

where k is a scalar gain and Ω is a diagonal, positive-definite matrix that assigns relative weights to the outputs. As a convention, we limit the magnitude of the elements in Ω to be between 0 and 1.

3.2 Centralized Analysis. Our system is a hybrid system, with multiple dynamic regimes and switching behaviors. Because each regime has a conserved energy $(E_{\text{heel}}, E_{\text{flat}}, E_{\text{toe}})$, we can define corresponding storage functions $(S_{\text{heel}}, S_{\text{flat}}, S_{\text{toe}})$ and control laws $(u_{\text{heel}}, u_{\text{flat}}, u_{\text{toe}})$. All other parameters are identical

between the controllers. The switching strategy is that when the dynamics switch contact configuration, the control is correspondingly switched. Our analysis applies to all of the continuous regimes, so we drop the subscripts for generality.

The convergence behavior in the continuous dynamics can be investigated by substituting the control law into the time-derivative of the storage function to get

$$\begin{aligned}\dot{S} &= -ky^\top \Omega\, y \\ &= -(E - E_{\text{ref}})^2 \dot{q}^\top B_u k \Omega B_u^\top \dot{q} \\ &= -2kS||\dot{q}||_\Omega^2\end{aligned} \tag{14}$$

where

$$||\dot{q}||_\Omega^2 = \dot{q}^\top B_u \Omega B_u^\top \dot{q} \tag{15}$$

is the square of a weighted norm. If we make the assumption that $||\dot{q}||_\Omega^2 \geq \eta \geq 0$, then

$$S(t) \leq S(0)e^{-2k\eta t} \tag{16}$$

which implies a minimum exponential convergence of the storage function, as long as the bound η holds.

One of the beneficial properties of PBC is that it is easy and natural to extend these results to the case of actuator saturation. Consider a saturated version of the control

$$u = \text{sat}(-k(E - E_{\text{ref}})\Omega B_u^\top \dot{q}) \tag{17}$$

This changes Eq. (14) to

$$\dot{S} = -ky^\top \Omega\, \text{sat}(y) \leq 0 \tag{18}$$

and the resulting system is still passive because the function output preserves the sign of the input, similar to the results in Ref. [30].

The main contribution of this derivation and analysis is to generalize similar results from Spong et al. [29] in two ways: to systems that already have a feedback controller (the inner loop here) and to systems with an arbitrary degree of underactuation.

Remark 1. The derivation of the control based on a conserved generalized system energy Eq. (5) gives a justification for why the PBC should work in conjunction with a pre-existing feedback controller. If the system is on the limit cycle, the energy is always equal to the reference energy and the PBC is always zero. Thus, the behavior of the system on the limit cycle is preserved in the presence of the PBC. However, it is important to note that the convergence of the system's generalized energy to the reference energy does not necessarily mean the biped is on the desired limit cycle (i.e., the walking gait). LaSalle's theorem in Ref. [29] only guarantees local asymptotic stability of the walking trajectory in the continuous dynamics. The condition $\dot{S} \equiv 0$ can produce multiple invariant sets that are locally asymptotically stable, including both sets where $E - E_{\text{ref}} \equiv 0$ and sets where $||\dot{q}||_\Omega^2 \equiv 0$. Furthermore, the form of these invariant sets is dependent on the biped model and the inner-loop control inputs v. For example, a stationary biped could be one of these invariant sets because $||\dot{q}||_\Omega^2 \equiv 0$.

Remark 2. The way the Ω-norm Eq. (15) enters into the storage function relation Eq. (14) gives a justification for why the controller should function with arbitrary underactuation. The fundamental relationship between the storage function and its derivative is always the same regardless of degree of underactuation. The only thing that changes is the bound η, which should increase with an increase in the number of actuators. From Eq. (16), we can see that this means more actuators cause an increase in the convergence rate of the storage function. However, more actuators and increased convergence speed are not always better. The basin of attraction of the limit cycle is shaped by every parameter that enters into the dynamics, in particular the choices of k, Ω, and B_u. In Sec. 3.3.3, we demonstrate the importance of these parameter choices in simulation and show that an increase in the number of actuators can actually lead to a degradation of performance.

So far, we have not analyzed the passivity and stability of the full hybrid system. There are several different notions of hybrid passivity that guarantee stability [31,32]. These notions rely on showing that the jump in storage caused by the discrete dynamics is bounded by the product of the input and output in some manner. This is somewhat difficult to show analytically for our biped system, since an impact can increase the storage function by lowering the energy below the reference energy. However, if the storage decreases between periods of the same contact configuration (e.g., the second instance of the heel phase has less storage than the first), then the hybrid dynamics converge to the reference energies.

The behavior of the jumps depends on both the continuous and discrete dynamics, and can be analyzed using the linearization of the Poincaré return map, $P(q, \dot{q})$, as in Ref. [3]. This map takes a postjump point $x_L = [q_L^+; \dot{q}_L^+]$ at the beginning of step L and maps to the next postjump point at step $L + 1$

$$x_{L+1} = P(x_L) \tag{19}$$

If this map has a fixed point, then there exists an associated limit cycle and conserved generalized system energy. For our multiphase hybrid system, one can use a single linear approximation of the map to confirm the local stability of the entire system numerically [3]. We do this in the following simulation section.

3.3 Centralized Simulations. This section offers simulations to exemplify how the centralized PBC affects the qualitative behavior of the biped system and demonstrate the analysis methods we use to quantify performance. A nominal limit cycle was found in Ref. [21] for a walking gait down on a slope of $\alpha = 0.095$ radians. This limit cycle is used to determine the reference energies for the PBC. The exact parameters used in the biped model and in the PD control are specified in Table 1, which are adopted from Ref. [21] and are human inspired. The PBC is applied as an

Table 1 Model parameters

Parameter	Variable	Value
Hip mass	m_h	31.73 (kg)
Thigh mass	m_t, m_{st}	9.457 (kg)
Shank mass	m_s, m_{ss}	4.053 (kg)
Foot mass	m_f, m_{sf}	1 (kg)
Thigh moment of inertia	I_t, I_{st}	0.1995 (kg/m^2)
Shank moment of inertia	I_s, I_{ss}	0.0369 (kg/m^2)
Full biped thigh length	l_t, l_{st}	0.428 (m)
Full biped shank length	l_s, l_{ss}	0.428 (m)
Full biped heel length	l_a, m_{sa}	0.07 (m)
Full biped foot length	l_f, l_{sf}	0.2 (m)
Hip equilibrium angle	$\bar{\theta}_h$	–0.5 (rad)
Hip proportional gain	K_{ph}	182.250 (N·m/rad)
Hip derivative gain	K_{dh}	35.100 (N·m s/rad)
Swing knee equilibrium angle	$\bar{\theta}_{\text{sk}}$	0.2 (rad)
Swing knee proportional gain	K_{psk}	182.250 (N·m/rad)
Swing knee derivative gain	K_{dsk}	18.900 (N·m s/rad)
Swing ankle equilibrium angle	$\bar{\theta}_{\text{sa}}$	–0.25 (rad)
Swing ankle proportional gain	K_{psa}	182.250 (N·m/rad)
Swing ankle derivative gain	K_{dsa}	0.810 (N·m s/rad)
Stance ankle equilibrium angle	$\bar{\theta}_a$	0.01 (rad)
Stance ankle proportional gain	K_{pa}	546.750 (N·m/rad)
Stance ankle derivative gain	K_{da}	21.278 (N·m s/rad)
Stance knee equilibrium angle	$\bar{\theta}_k$	–0.05 (rad)
Stance knee proportional gain	K_{pk}	546.750 (N·m/rad)
Stance knee derivative gain	K_{dk}	21.278 (N·m s/rad)

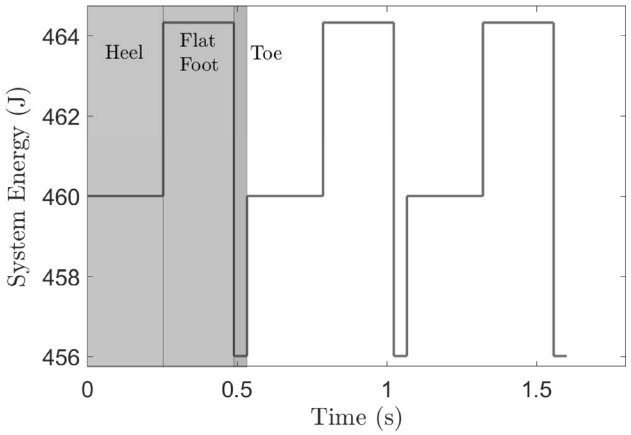

Fig. 2 Generalized energy (*E*) of the PD controlled (inner-loop) biped system while traversing the limit cycle. There are three constant energy levels with discrete jumps between them.

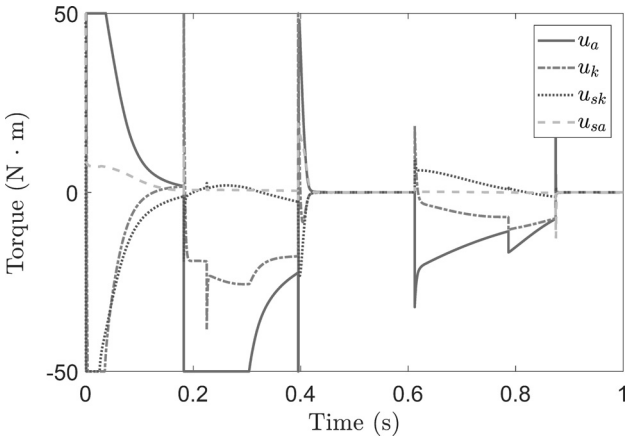

Fig. 4 Torque over time for the centralized controller *U* for the first three steps

outer loop of the PD control (inner loop). Since p_x and p_y are always constrained to the ground, the biped is fully actuated during the flat foot phase and underactuated with degree one during heel and toe contact due to ϕ. The entries in the diagonal vector for Ω that correspond to p_x, p_y, and ϕ are always zero since they are unactuated. The PBC is always saturated at 50 N·m, as a reasonable limit of the physical capability of the actuators on an exoskeleton [12].

The PD controlled biped has three contact configurations, which cause the nominal limit cycle to transition between three different constant system energies, $E_{\text{heel}} \rightarrow E_{\text{flat}} \rightarrow E_{\text{toe}}$. This can be seen in the periodic, constant jumps in Fig. 2, which shows the trajectory for the generalized energy $E = K + P - W$ versus time, for three steps. The jumps are an artifact caused by the physical decrease in kinetic energy due to an impact, the shift of the virtual potential energy datum between different locations on the biped, and the reset of the work integral between steps. The three distinct energies E_{heel}, E_{flat}, and E_{toe} are used as the reference values for the centralized PBC during the corresponding contact constraint.

3.3.1 Storage Convergence. When the system is solely under the influence of the PD controller, the storage function S and system energy E remain constant during the continuous dynamics, and are only changed by the discrete dynamics (i.e., impacts). Implementing the PBC on top of the PD controller qualitatively changes the system behavior by forcing the storage function to converge during the continuous dynamics as well. This is demonstrated in Fig. 3, which gives the storage over time of the biped system perturbed by $\Delta x_o = [0_{8\times1}; 0.4\,\dot{q}_o]$. Here, the control parameters $\Omega = [0, 0, 0, 1, 1, 0.001, 1, 1]I_{8\times8}$ and $k = 1$ were chosen for simplicity and to respect the physical symmetry of the biped. Similar to Fig. 2, the discrete jumps in the storage are caused by the impact dynamics. The storage decreases between periods of the same contact configuration (e.g., the second instance of the heel phase has less storage than the first) with or without PBC, which is important for the notion of hybrid passivity from Ref. [31]. The convergence of the storage function during the continuous dynamics appears to be exponential for the PBC case, with different rates for each contact condition. This result is expected based on Eq. (16). The effect of this behavior is that the centralized PBC forces the storage close to zero in five steps, which is much faster than the PD control alone. If we consider the storage as a metric for how close the biped is to the nominal limit cycle, then we can conclude that the PBC causes the biped to reach steady-state walking faster. However, the storage only gives an indication of convergence speed. It does not definitively demonstrate stability of the hybrid limit cycle nor does it demonstrate a notion of robustness; these ideas are discussed in Sec. 3.3.3.

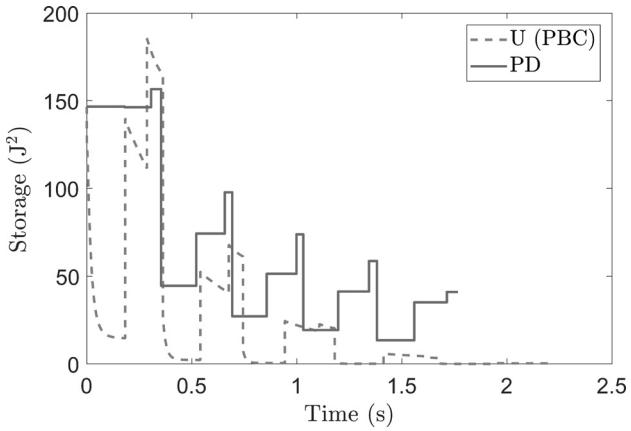

Fig. 3 Centralized storage function for the perturbed system with PBC and without PBC, over five steps. The transition between steps is marked by a large decrease in storage, caused by heel impact.

3.3.2 Control Torques. The torques of PBC for the first three steps of the simulation from Fig. 3 are given in Fig. 4. The specific joint where the control torque u_i acts is indicated by the subscript $i \in \{\text{a}, \text{k}, \text{h}, \text{sk}, \text{sa}\}$. The figure indicates that the saturation effect does significantly influence the torque profile, especially for the stance ankle actuator. It is interesting to note that the torques for the stance leg are generally larger than those for the swing leg; this is because the velocities of the joints in the swing leg are smaller in general. The torque trajectory in the first phase has an exponential like trajectory for all the joints, which corresponds to the exponential convergence of the energy to the reference since the torque is proportional to this term. When the energy error becomes small enough, the dynamics of the joint velocities begin to have a larger influence on the control torques. Again, the jumps in the control torque are caused by the instantaneous changes in velocity and energy at impact.

3.3.3 Stability and Robustness. At the end of Sec. 3.2, we stated that the stability of the limit cycle of the hybrid system can be determined by calculating the eigenvalues of the linearized Poincaré map. If the eigenvalues Λ of the linearization lie within the unit circle, then the limit cycle is locally exponentially stable [3]. Figure 5 displays the largest magnitude of all the eigenvalues as k is varied from 0 to 10 with $\Omega = [0, 0, 0, 1, 1, 0.001, 1, 1]I_{8\times8}$. This single value is displayed for clarity and conciseness because the linearization has 16 eigenvalues. The figure indicates that the

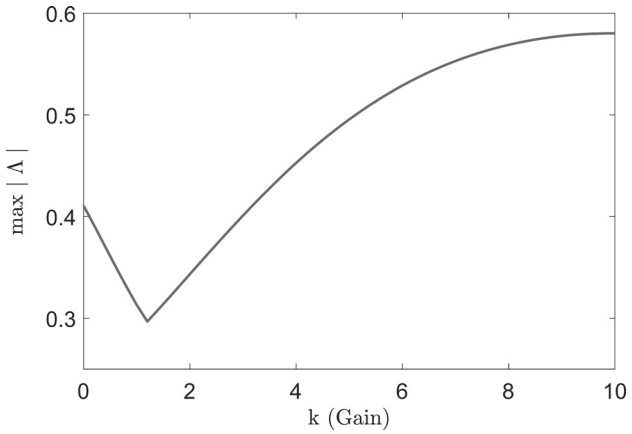

Fig. 5 Maximum absolute value of the eigenvalues of the linearization of the Poincaré map as the gain *k* is varied from 0 to 10

system is stable for this range of gains since the value is always less than one.

The linearization of the Poincaré map can give some notion of robustness, namely the margin from largest eigenvalue to the unit circle (basically a gain margin). However, there is not a consensus in the field of biped locomotion on what exactly "robustness" means. Many researchers use the eigenvalues as described and say that an increased margin indicates a more robust walking gait [33,34]. This has drawbacks, namely that eigenvalues characterize local stability and rate of convergence; they contain little information about global properties of the nonlinear system like basin of attraction or robustness. Furthermore, sensitivity to numerical error can result in unstable eigenvalues for a stable orbit (an effect we saw while working with these simulations). A more thorough discussion of the robustness of walking bipeds exists in other works [35,36]. Because of these issues, we turn to a modification of this metric.

A metric called the "gait sensitivity norm," with the notation $||\partial g/\partial e||_2$, was proposed in Ref. [36] to provide a measure of the robustness of bipedal gait. It has been subsequently utilized in several other works [37–39]. We use it to compare the effectiveness of the different PBCs in our simulations by considering an increase in $1/||\partial g/\partial e||_2$ as an increase in robustness. The calculation of this norm requires gait indicators, gait perturbations, and a linearization of the Poincaré return map. The indicators are essentially failure modes of the system and the perturbations are characteristic of actions on the system that cause failure. We regard "failure" as the biped ceasing to walk. The gait indicators are step length, step time, and the minimum ground clearance of the swing leg heel over the duration of midstance. The disturbances are a change of slope by ± 1 radian and a perturbation vector $\Delta x_o = [0_{8\times1}; 0.4\,\dot{q}_o]$ that introduces a scaled initial velocity at heel strike. We calculate the Poincaré return map [3] at heel strike after three steps in our analysis. Based on our choice of indicators and perturbations, we can interpret limit cycles with "better" gait sensitivity norms as being robust to changes in ground slope and velocity disturbances, in the sense that they are farther away from the minimum "allowable" indicator values.

The nominal limit cycle of biped system under PD control alone has a reciprocal norm of $1/||\partial g/\partial e||_2 = 0.1584$. The biped with the centralized PBC with the parameters used to generate Fig. 3 has a reciprocal norm of $1/||\partial g/\partial e||_2 = 0.0248$, which indicates a less robust system. This might seem to indicate that the PBC cannot achieve the goal of improving the robustness of the biped. However, by simply changing the PBC parameters to $\Omega = [0, 0, 0, 1, 1, 0.001, 1, \mathbf{0}]I_{8\times8}$ (removing the PBC actuator at the swing ankle and keeping everything else the same), we find an increase in robustness with $1/||\partial g/\partial e||_2 = 0.6341$. This demonstrates that it is important to judiciously choose values in Ω. To understand why such a dramatic change occurs, consider an edge case when $\Omega = [0, 0, 0, 0, 0, 0, 0, \mathbf{1}]I_{8\times8}$. Essentially, this causes the swing foot to act as a reaction wheel pendulum in a similar manner to Ref. [30]. Since the impact map is extremely sensitive to the state of the swing foot at impact, this control parameter choice contracts the basin of attraction of the desired limit cycle dramatically. This causes the biped to fall over when the generalized energy is slightly perturbed.

4 Decentralized Passivity-Based Control

The controller in Sec. 3 relies on the ability to measure all inertial and geometrical properties of the biped. It also relies on measuring all the joint positions and velocities, inner loop torques, and external forces applied to the system in order to continuously calculate the generalized system energy. In the context of the application to a powered prosthesis or exoskeleton, one generally has an accurate model of the powered device and rough estimates of the user's mass distribution and geometry. The biggest challenge relates to the inability to measure all of the user's joint velocities and torques. The straightforward approach might seem to be to partition the system into user and device [20], and then use the energy of the device to construct a PBC. However, we can improve upon this with a partitioning scheme that utilizes all the available model parameter and state information to construct a PBC that is robust to parametric error.

4.1 Decentralized Derivation. The set of model parameters Θ contains all of the mass, inertia, and link length parameters of the biped given in Eq. (1). From this, the set of measured parameters $\Theta_O \subset \Theta$ can be constructed to collect all of the model parameters that are available in the design of the PBC. Note that the subset Θ_O can also contain mass, inertia, and link length parameters. Similarly, a vector of measured states $x_O = [q_O; \dot{q}_O] \in \mathrm{R}^{2\mathrm{b}\times1}$ can be extracted from the state vector $x = [q; \dot{q}]$, where the vectors of measured position and velocity variables are $q_O \in \mathrm{R}^{\mathrm{b}\times1}$ and $\dot{q}_O \in \mathrm{R}^{\mathrm{b}\times1}$, respectively. The number of joints with position and velocity measurements is given by b.

Equipped with Θ_O and x_O, we can use them to find a subexpression in the Lagrangian of the mechanical system $\mathcal{L}(x, \Theta) = K - P$ that represents the measurable subsystem $\mathcal{L}_O(x_O, \Theta_O)$ such that

$$\mathcal{L} = \mathcal{L}_O + \mathcal{L}_{\bar{O}} \tag{20}$$

where $\mathcal{L}_{\bar{O}}$ is an unmeasured or unmodeled part of the system that cannot explicitly enter into the controller. To do this, we proceed by finding a subexpression $K_O(q_O, \dot{q}_O, \Theta_O)$ for the kinetic energy and $P_O(q_O, \Theta_O)$ for the potential energy such that $\mathcal{L}_O(q_O, \dot{q}_O, \Theta_O) = K_O - P_O$.

The kinetic energy of the biped system is

$$K = \frac{1}{2}\dot{q}^\top M(q, \Theta)\dot{q} \tag{21}$$

The mass matrix M in the expression for K can be calculated using the method from Ref. [23] as

$$M = \sum_{\mathrm{j}=1}^{n} J_{\mathrm{j}}^\top(q)\mathcal{M}_{\mathrm{j}}J_{\mathrm{j}}(q) \tag{22}$$

This method constructs the mass matrix link by link, where $J_{\mathrm{j}} \in \mathbb{R}^{6\times n}$ and $\mathcal{M}_{\mathrm{j}} \in \mathbb{R}^{6\times6}$ are the body Jacobian and generalized inertia matrix of the jth link, respectively. The mass matrix can be partitioned into

$$M = \Psi + M_O(q_O, \Theta_O) \tag{23}$$

$$M_O = \sum_{\mathrm{j}=1}^{n} J_{\mathrm{j}O}^\top \mathcal{M}_{\mathrm{j}O} J_{\mathrm{j}O} \tag{24}$$

where $M_O(q_O, \Theta_O)$ is a modified mass matrix that collects additive terms in M that are functions of the symbols in Θ_O and x_O, exclusively. As it will be shown, M_O is constructed by obtaining a modified body Jacobian $J_{\mathrm{i}O}(q_O, \Theta_O)$ and a modified inertia matrix $\mathcal{M}_{\mathrm{i}O}(\Theta_O)$ for each link through a partitioning scheme. The remainders of the terms from this scheme are all collected in the variable Ψ, and we make no claims about its properties.

The matrix $\mathcal{M}_{\mathrm{i}}$ is always positive definite by construction because it has the form

$$\mathcal{M}_{\mathrm{i}} = \mathrm{diag}(m_{\mathrm{i}}, m_{\mathrm{i}}, m_{\mathrm{i}}, I_{\mathrm{i}xx}, I_{\mathrm{i}yy}, I_{\mathrm{i}zz}) \tag{25}$$

which contains on the diagonal the mass and the inertias about the principal axes of the link. It can be decomposed into

$$\mathcal{M}_{\mathrm{i}} = \mathcal{M}_{\mathrm{i}O} + \mathcal{M}_{\mathrm{i}\bar{O}} \tag{26}$$

where $\mathcal{M}_{\mathrm{i}O}$ is a diagonal matrix that extracts all the symbols in $\mathcal{M}_{\mathrm{i}}$ that are also in Θ_O. It is important to note that any $\mathcal{M}_{\mathrm{i}O}$ is positive semidefinite as long as $\mathcal{M}_{\mathrm{i}}$ contains at least one symbol in Θ_O. The remainder $\mathcal{M}_{\mathrm{i}\bar{O}}$ is collected into Ψ. Now, all that remains is to partition the body Jacobian.

In general, each element $\mathrm{e}_{i,k}$ in J_{i} has the form

$$\mathrm{e}_{i,k} = \sum_{z=1}^{n} \mathrm{d}_z\, l_z f_z(q_z) = \sum_{z=1}^{n} T_z \tag{27}$$

based on Ref. [23]. The coefficient d_z takes values between zero and one depending on where the center of mass of the jth link is relative to the rest of the kinematic chain, while l_z is an arbitrary link length in Θ. The function f_z depends on a vector of position state variables q_z, the exact form of which depends on the type of joints (revolute or prismatic) that make up the kinematic chain. We partition each element into

$$\mathrm{e}_{i,k} = \mathrm{e}_{Oi,k} + \mathrm{e}_{\bar{O}i,k} \tag{28}$$

where $\mathrm{e}_{Oi,k}$ is the summation of the terms T_z where $l_z \in \Theta_O$ and q_z is a symbol in x_O. The term $\mathrm{e}_{\bar{O}i,k}$ is collected into the remainder Ψ.

The body Jacobian matrix can then be partitioned element-by-element so that $J_{\mathrm{i}O}$ is constructed from the $\mathrm{e}_{Oi,k}$ elements. Thus, we have demonstrated the methods for constructing the $J_{\mathrm{i}O}$ and $\mathcal{M}_{\mathrm{i}O}$ terms in Eq. (24). As previously noted, each $\mathcal{M}_{\mathrm{i}O}$ is positive semidefinite, which implies M_O is also positive semidefinite.

By substituting Eqs. (23) into (21), the kinetic energy can be written as

$$K = \frac{1}{2}\begin{bmatrix}\dot{q}_O^\top & \dot{q}_{\bar{O}}^\top\end{bmatrix}(M_O + \Psi)\begin{bmatrix}\dot{q}_O \\ \dot{q}_{\bar{O}}\end{bmatrix} \tag{29}$$

We can construct the subexpression K_O, which retains a quadratic form of

$$K_O = \frac{1}{2}\begin{bmatrix}\dot{q}_O^\top & 0\end{bmatrix}M_O\begin{bmatrix}\dot{q}_O \\ 0\end{bmatrix} \tag{30}$$

so that $K_O \geq 0$. This means that K_O can be treated as the kinetic energy of a subsystem.

Similarly, we can partition the potential energy into two components. To see this, consider the definition for the potential energy

$$P(q) = \sum_{n=1} m_{\mathrm{i}} h_{\mathrm{i}}(q, \Theta) g \tag{31}$$

It is also possible to partition this energy into

$$P = P_O(q_O, \Theta_O) + P_{\bar{O}} \tag{32}$$

by extracting the terms in the summation that belong to q_O and Θ_O. Since P depends only on position state information, any subexpression P_O will also depend on only position state information and as such can be considered a new potential energy. Thus, the subexpression $\mathcal{L}_O$ is Lagrangian and defines a Lagrangian subsystem. The dynamics of this system are

$$\begin{aligned} &M_O(q_O, \Theta_O)\ddot{q}_O + C_O(q_O, \dot{q}_O, \Theta_O)\dot{q}_O + N_O(q_O, \Theta_O) \\ &\quad = \Gamma(q, \dot{q}, \Theta, v, u_O) + B_O u_O \end{aligned} \tag{33}$$

where $M_O \in \mathrm{R}^{b\times b}$ is the mass matrix for the subsystem, $C_O \in \mathrm{R}^{b\times b}$ is the corresponding Coriolis/centrifugal matrix, and $N_O \in \mathrm{R}^{b\times 1}$ is a gravitational force vector. Torques generated by both the interaction with the unmodeled system $\mathcal{L}\bar{O}$ and the inner loop control v are represented by Γ, while the torques applied by local actuators and their mapping into the subsystem are represented by the term $B_O u_O$.

A generalized energy can be defined for this subsystem and used in a constructive analysis, similar to Sec. 3, to arrive at a decentralized PBC for the subsystem. We begin with

$$E_O(q_O, \dot{q}_O, \Theta_O, \Gamma, t) = K_O + P_O - W_O(q_O, \dot{q}_O^\top, \Gamma, t) \tag{34}$$

where

$$W_O = \int_0^t \dot{q}_O^\top \Gamma\, d\tau \tag{35}$$

and define a storage function for the decentralized subsystem as

$$S_O(q_O, \dot{q}_O, \Theta_O, \Gamma, t) = \frac{1}{2}(E_O - E_{O\mathrm{ref}})^2 \tag{36}$$

Then, we follow the procedure applied in Sec. 3.1 to go from Eqs. (7) to (13). We take the time-derivative of S_O to find

$$\dot{S}_O = (E_O - E_{O\mathrm{ref}})(\dot{E}_O - \dot{E}_{O\mathrm{ref}}) \tag{37}$$

and E_O to find

$$\begin{aligned} \dot{E}_O &= \frac{d(K_O + P_O)}{dt} - \frac{dW_O}{dt} \\ &= \left(\dot{q}_O^\top B_O u_O + \dot{q}_O^\top \Gamma\right) - \dot{q}_O^\top \Gamma \end{aligned} \tag{38}$$

$$= \dot{q}_O^\top B_O u_O \tag{39}$$

which follows from Eqs. (33) to (35). By substituting $\dot{E}_O$ into $\dot{S}_O$, we find

$$\dot{S}_O = (E_O - E_{O\mathrm{ref}})(\dot{q}_O^\top B_O u_O - \dot{E}_{O\mathrm{ref}}) \tag{40}$$

Upon inspection of $\dot{E}_O$, it is apparent that the generalized energy does indeed take a constant value on the limit cycle, since $\dot{E}_O = 0$ when $u_O = 0$. This means $\dot{E}_{O\mathrm{ref}} = 0$ on the limit cycle for the uncontrolled subsystem. Thus, we can define a decentralized controller

$$u_O(q_O, \dot{q}_O, \Theta_O, \Gamma, t) = -k_O \Omega_O (E_O - E_{O\mathrm{ref}}) B_O^\top \dot{q}_O \tag{41}$$

with similar passivity, saturation, and exponential convergence properties to the centralized case.

4.2 Decentralized Analysis. The dynamics of the decentralized system indicate that the control is robust to parametric error, which can be realized by considering the partitioning schemes for Eqs. (26) and (27). The parametric error can be captured by a set Θ_e, where each element $\theta_e \in \Theta_e$ is the difference between an

estimated parameter and the true parameter. This implies the generalized inertia tensor $\mathcal{M}_{\hat{}}$ and the body Jacobian element $j_{i,k}$ will have corresponding error terms. However, if we use the estimated parameters in the partitioning scheme, then the errors will be absorbed into the remainder term Ψ and will propagate into the decentralized dynamics through Γ. By Eq. (39), the generalized energy for this system with error will still have a conserved value along the limit cycle. Essentially, the estimated parameters can be used to determine and track the subsystem reference energy, regardless of parametric error.

One of the interesting properties of this decentralized controller is that it has immediate implications for the storage function of the centralized system. This controller ensures convergence of the decentralized system to the target reference energy $E_{O\text{ref}}$, but it also makes the storage function for the *centralized* system converge to some finite energy value that emerges due to the new dynamics. This is because u_O can be considered as a passive input to both systems, which implies $\dot{E}_O = \dot{E}$. Thus, in the continuous dynamics $E_O \to E_{O\text{ref}}$ as $u_O \to 0$, and E will converge to some steady-state error relative to E_{ref}. When $u_O = 0$, the biped is still under the influence of the inner loop control v, and still has a stable limit cycle. Therefore, the discrete dynamics should cause $E \to E_{\text{ref}}$ as seen in Fig. 3.

4.3 Decentralized Simulations. This section explores the behavior of the biped with two different decentralized PBCs while comparing them among each other, to the centralized PBC, and to the biped with only PD control. The motivation behind these comparisons is to gain an understanding for the potential application to an exoskeleton. The centralized PBC represents the theoretical case if we could get perfect measurements of the human parameters and motion, while the decentralized cases represent the compromise made by the choice of the system model. The PD control alone represents the human walking without any assistance. Again, all the PBC controllers were saturated at 50 N·m.

We have the two decentralized controls U_ζ, U_ξ and the centralized control U. The main difference between the two decentralized controls is the model information that they use. Specifically, U_ζ utilizes the same full model parameter set Θ as the centralized control U, but it restricts the state information to a vector x_O local to the stance leg such that

$$x_O = [p_x, p_y, \phi, \theta_a, \theta_k, \dot{p}_x, \dot{p}_y, \dot{\phi}, \dot{\theta}_a, \dot{\theta}_k]^\top \tag{42}$$

The second decentralized PBC U_ξ uses the restricted state information x_O and also uses a restricted model parameter set

$$\Theta_O = \{m_f, m_s, I_f, I_s, l_f, l_s\} \tag{43}$$

that is also local to the stance leg. This is essentially modeling the stance leg as a completely separate subsystem. This gives rise to subsystems with generalized energies $E_\zeta(x_O, \Theta)$ and $E_\xi(x_O, \Theta_O)$ that are used to construct the controls U_ζ and U_ξ, respectively. The energy E_ξ has a physical interpretation: it is the energy of the stance shank and foot. The energy E_ζ does not have such an intuitive meaning.

In order to implement the decentralized controllers U_ζ and U_ξ, we need target reference energies for each of them at each contact configuration. These can be found in simulation by simply computing the value of their generalized energies over the nominal limit cycle of the biped under PD control alone. We see in Fig. 6 that the decentralized energies take constant values on the limit cycle, as expected. Since the construction of E_ξ ignores the majority of the mass and inertia terms of the biped system, it is expected that its value along the limit cycle is significantly smaller compared to the other two energies. In contrast, when E_ζ is compared to the real system energy E, it has an increased virtual potential energy, which makes it larger than E.

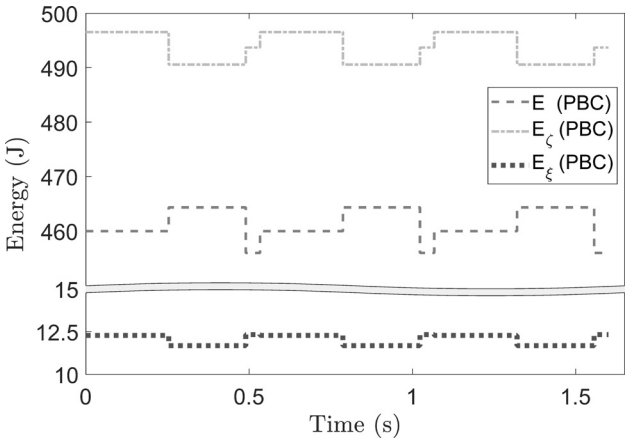

Fig. 6 Generalized energy of all three systems while traversing the limit cycle. There is a break in the *y*-axis of the graph to accommodate the difference in average magnitude of the energy trajectories.

4.3.1 Storage Convergence. We constructed an experiment of four simulations with a perturbation to the biped's initial condition on the limit cycle. The independent variable is the control method used in each simulation. The control parameters for all three PBC controllers were kept the same, with $\Omega = [0, 0, 0, 1, 1, 0, 0, 0]I_{8\times 8}$ and $k = 1$, which limits actuation to the stance side knee and ankle. The same perturbation to the state of the biped on the limit cycle at heel strike $\Delta x_o = [0_{8\times 1}; 0.4\,\dot{q}_o]$ was used in each simulation. Since the point of introducing control into the system is to make the *entire* biped system converge back to the limit cycle, we examined the *centralized* storage function that utilizes the full state and model parameter information. By contrast, the storage function of one of the decentralized systems only gives information about the convergence of a portion of the biped.

From Fig. 7, we can see that the behavior for the PBC U_ξ is very close to the system with PD control only, while the decentralized PBC U_ζ is very close to the "best case" scenario of the centralized system. Again, the convergence rate back to the limit cycle is significantly faster for U and U_ζ than for U_ξ and PD control alone. This confirms that there a gain in performance from the partitioning scheme in Sec. 4 to generate U_ζ rather than simply modeling the stance leg as a localized subsystem to generate U_ξ. The decentralized control U_ζ does not converge quite as quickly as U, but this is to be expected since it does not utilize the full state feedback.

This plot exemplifies the points made in Secs. 6 and 5 about the connections between the implementation method and storage

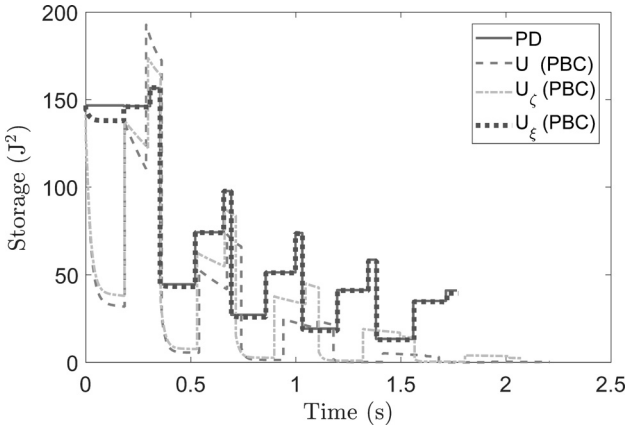

Fig. 7 System storage function across PBC implementations

Table 2 Reciprocal of the gait sensitivity norm calculated across controllers and scaling gains

Reciprocal of gait sensitivity norm $(1/\|\|\partial g/\partial e\|\|_2)$			
	$k=0.01$	$k=1$	$k=10$
U	0.1614	0.6614	3.0454
U_ζ	0.1594	0.3345	2.2086
U_ξ	0.1584	0.1597	0.1755
PD		0.1584	

injection. The reason why the decentralized control U_ξ essentially acts like the biped with PD control alone is because the magnitude of the energy error is small compared to the other PBCs. This means less storage is injected to the system at each impact and since this storage does not accurately account for the "real distance" to the limit cycle, the control is less effective. The decentralized PBC U_ξ resembles the performance of to the centralized control U precisely because the generalized energy for that decentralized subsystem is close to the centralized energy.

4.3.2 Robustness. The robustness properties of each system are characterized by the gait sensitivity norm. We performed a simulation experiment to examine this across an array of different scaling gains k for each control while maintaining the same weighting matrix $\Omega = [0,0,0,1,1,0,0,0]I_{8\times8}$. This allows a rigorous comparison of the robustness of the different controls. The results of this experiment are displayed in Table 2. This table demonstrates the same relationship observed in the storage analysis; that U and U_ζ are similar in behavior while U_ξ acts more like PD control alone. Also, there is a strict ordering of the control methods across all the selected gains, in terms of robustness, that correlates with the amount of information available to the control. In other words, utilizing a larger information set to construct the PBC makes the biped more robust. While the table seems to indicate that increasing the scaling gain always makes the gait more robust, this is not always the case. For example, increasing the gain of the centralized control to $k=100$ makes the reciprocal of the gait sensitivity norm $1/\|\|\partial g/\partial e\|\|_2 = 2.0055$, and increasing further still to $k=1000$ makes $1/\|\|\partial g/\partial e\|\|_2 = 0.001$, which is a large decrease in robustness. These results reveal that there exists a limit on the scaling gain such that exceeding the limit actually makes the system performance worse.

4.4 Model Parameter Error. In this section, we explore the effect of parameter error in the energy function of the decentralized control U_ζ. Based on the results in Sec. 4.3, this control

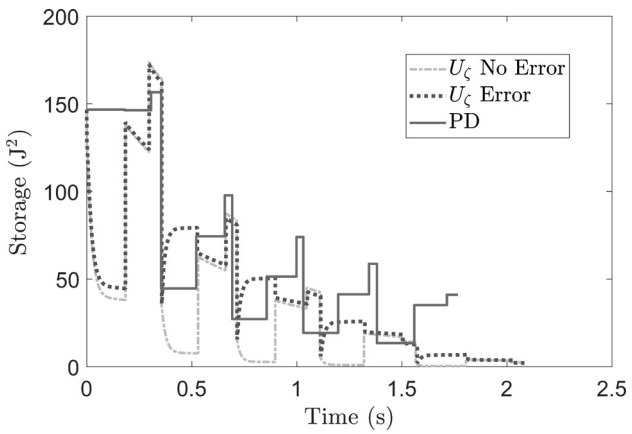

Fig. 8 System storage function for a decentralized PBC with perfect model parameters versus a decentralized PBC with random ±30% error in the model parameter

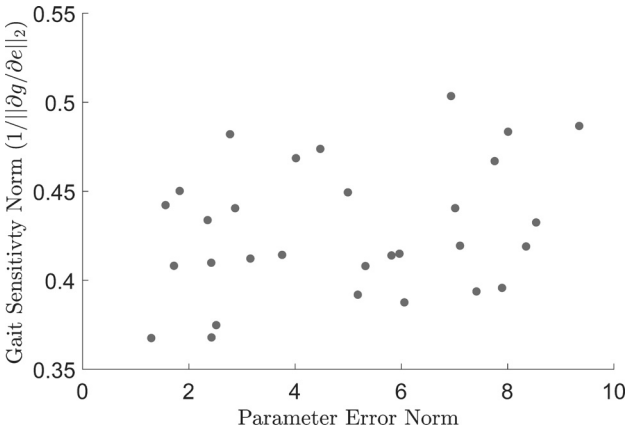

Fig. 9 Robustness of decentralized control versus model parameter error norm with $k=1$

represents the best version that could be implemented on a wearable device. However, it is practically guaranteed that measures or estimates of the inertia of the user will have some error. Furthermore, we believe that the characteristics of the parameter error in this scenario should generalize to the other control cases based on the analysis at the end of Sec. 4 and results in Sec. 4.3. An example simulation is given in Fig. 8 that uses U_ζ with control parameters $\Omega = [0,0,0,1,1,0,0,0]I_{8\times8}$, $k=1$, and a set of arbitrarily chosen model parameter errors of ±30% difference from the parameters in Θ. It is perturbed off the limit cycle at heel strike by $\Delta x_o = [0_{8\times1}; 0.4\dot{q}_o]$. It is important to note that the reference energies are calculated with the inaccurate model parameters and then used in the control with the same error. This method ensures the storage function is zero along the limit cycle and also is reflective of a real-world implementation.

Even with model parameter error, the decentralized control still causes the biped to converge to the limit cycle in less steps than without PBC, as seen in Fig. 8. During heel contact of the second and third step, it seems that the storage function is larger than the non-PBC case but this behavior is transient and quickly disappears. In addition, the value of the reciprocal gait sensitivity norm for the control with parameter error is $1/\|\|\partial g/\partial e\|\|_2 = 0.6614$, which is greater than the non-PBC system.

To investigate the general behavior of the PBC under model parameter error, we ran an experiment with consistent control parameters where we calculated the gait sensitivity norm for the system with 30 random sets of model parameter errors. The error multiple for each parameter $\mu \in \Theta$ was a uniform random variable in ±0.3, and we calculated the parameter error norm as the two-norm of all these error values. A scatter plot of the results is given in Fig. 9. All of the values on the plot are significantly larger than the gait sensitivity norm for the PD control alone. These results support the idea discussed in Sec. 5, that as long as the scheme for calculating the storage injection at each impact correlates with the energy of the system, the control should make the system more robust. The major point of the experiment is to show the efficacy of the PBC under random parametric error and not some "cherry-picked" values.

5 Adaptive Reference Energy

In Sec. 3.1, an assumption about the magnitude of the velocity norm was given in order to bind the convergence of the storage function. This technical detail can be removed by utilizing a time-varying reference energy, as opposed to a constant reference energy, as seen in Ref. [40]. With this technique, the storage function remains the same though its time-derivative changes to

$$\dot{S} = (E - E_{\text{ref}})(\dot{q}^\top B_u u - \dot{E}_{\text{ref}}) \tag{44}$$

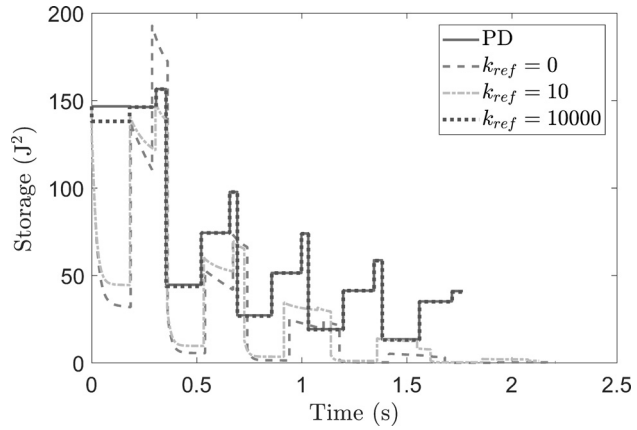

Fig. 10 System storage function for the centralized PBC with various adaptation gains. The scaling gain $k = 1$ is used across all cases. The PD control by itself is given for comparison.

In Ref. [40], the adaptation law for the reference energy is

$$\dot{E}_{\text{ref}} = k_{\text{ref}}(E - E_{\text{ref}}) \tag{45}$$

which when combined with the control law Eq. (13), results in

$$\dot{S} = (E - E_{\text{ref}})(-k||\dot{q}||^2_{\Omega}(E - E_{\text{ref}}) - k_{\text{ref}}(E - E_{\text{ref}})) \tag{46}$$

$$= (E - E_{\text{ref}})^2(-k||\dot{q}||^2_{\Omega} - k_{\text{ref}}) \tag{47}$$

where k_{ref} is an adaptation gain that can be utilized for design. This shows that even when $||\dot{q}||^2_{\Omega} = 0$, the storage function is bounded by

$$S(t) \leq S(0)e^{-2k_{\text{ref}}t} \tag{48}$$

which gives an absolute, deterministic convergence rate. However, the association of a *constant* reference energy with a *specific* desired limit cycle of the system is lost.

5.1 Adaptive Simulation. In this section, we explore the effect of the variation of the adaptation gain k_{ref} in a time-varying reference energy. As mentioned in Sec. 5, if the norm of the joint velocities becomes zero, then we lose the exponential convergence of the storage function, but this can be addressed by the time-varying energy. We choose to use the centralized U in these simulations, with parameters of $\Omega = [0, 0, 0, 1, 1, 0.001, 1, 0]I_{8\times 8}$ and $k = 1$. In Fig. 10, we show some example cases of the system with the perturbation $\Delta x_o = [0_{8\times 1}; 0.4\dot{q}_o]$ off the limit cycle at heel strike. The storage function in this figure uses the constant reference energies from Fig. 2, *not* the time-varying energy, in order for the storage to be a valid metric for convergence to the limit cycle. However, we stress that the control has an adaptive, time-varying reference energy as input. As the figure shows, having a high adaptation gain k_{ref} makes the system behave as if the PBC was inactive. This is because the adaptation causes the reference energy to converge to the current system energy very quickly without dissipating error from the original limit cycle. The figure also indicates the system converges back to the desired limit cycle regardless of the adaptation gain.

6 Discussion on Implementation

In the application to wearable devices, all of the control methods appear to require knowledge of human joint torques and/or the interaction forces between the user and the device. Distinguishing between forces caused by nominal walking behavior and forces caused by a disturbance is not a trivial task. However, here we suggest an implementation of the PBC that allows us to shortcut these challenges.

By considering the generalized system energy Eq. (5) and its derivative Eq. (10), we can rewrite the energy as

$$E = E_{\text{init}}(q^+, \dot{q}^+) + \int_0^t \dot{q}^\top B_u u \, dt \tag{49}$$

$$= E_{\text{init}} - k\int_0^t (E - E_{\text{ref}})\dot{q}^\top B_u \Omega B_u^\top \dot{q} \tag{50}$$

where E_{init} is the mechanical energy at $t = 0$, since $W(0) = 0$ by convention. Equation (49) implies that a PBC implementation could determine the value of E_{ref} on the limit cycle, update the postimpact mechanical energy E_{init} at each impact, and continuously measure the velocities $B_u^\top \dot{q}$ at the actuated joints. This method can be used for both the centralized and decentralized controllers.

The trade-off of this implementation is a loss of disturbance rejection in the continuous dynamics. As previously stated, this is caused by not accounting for torques generated outside of the PBC. However, external disturbances will cause a change in the pre-impact state, which should propagate to a change in the post-impact mechanical energy, which will change E_{init}. This indicates that the PBC will begin to react to the disturbance at the start of the next step.

The control implementation is equivalent to a scheme for injecting a finite amount of storage

$$S_{\text{init}}(q^+, \dot{q}^+) = \frac{1}{2}\left(E_{\text{init}}(q^+, \dot{q}^+) - E_{\text{ref}}\right)^2 \tag{51}$$

at impact and then allowing the control to dissipate it. The intuition behind the PBC is that this value should quantify the "distance" in the energy space to the desired limit cycle. Though we derive the method for calculating S_{init} based on a model, the decentralized analysis suggests that it is valid to use any metric that becomes zero on the desired limit cycle. It should also correlate with the system energy in such a way that the notion of hybrid passivity in Ref. [31] is preserved from one stride to the next (i.e., the impact dynamics dissipate the metric).

In addition, there are other schemes for choosing the postimpact storage update. For example, the method in Ref. [1] adds a term into S_{init} to push the biped toward a desired walking speed that is different from the original target limit cycle. It is well known that a biped's walking speed correlates with kinetic energy [9,41], which provides some intuition as to why this is effective. Since walking speed is only one feature of a walking gait, this idea could be extended to account for a wider variation of tasks in a neighborhood of a known limit cycle.

7 Conclusion

We conclude that a decentralized PBC can be generated that has performance close to the centralized control by maximizing the use of available state and model parameter information. We also show that control can improve the robustness and convergence of the biped to the limit cycle, even in the presence of model parameter error. This decentralization directly addresses the challenges introduced by the application to wearable devices, since the human user represents a highly complex unmodeled dynamical system. The control is also passive, which has been used in teleoperation [42] and has useful properties for the general domain of human–machine interaction by ensuring that the energy output of the system is bounded by the human input. This could help us design controllers for wearable robots that are responsive to the human input while also having confidence in the safety and stability of the device and user. One of the limitations of this work is the issue of implementation on a physical system. The

implementation method we suggest does not attempt to measure the external forces applied to the system in the continuous dynamics, which may limit the responsiveness of the control method. However, we believe that the method can still impart benefits, such as an increase in the basin of attraction. The authors plan to implement this method in hardware and perform physical experimentation as future work.

Acknowledgment

R. D. Gregg holds a Career Award at the Scientific Interface from the Burroughs Wellcome Fund.

Funding Data

- NSF (Grant No. CMMI-1652514; Funder ID: 10.13039/501100008982).
- National Institute of Child Health and Human Development of the NIH (Grant Nos. DP2HD080349 and R01HD094772; Funder ID: 10.13039/100000071).
- Burroughs Wellcome Fund (Funder ID: 10.13039/100000861).

References

[1] Goswami, A., Espiau, B., and Keramane, A., 1997, "Limit Cycles in a Passive Compass Gait Biped and Passivity-Mimicking Control Laws," Auton. Robots, **4**(3), pp. 273–286.

[2] Gupta, S., and Kumar, A., 2017, "A Brief Review of Dynamics and Control of Underactuated Biped Robots," Adv. Rob., **31**(12), pp. 607–623.

[3] Westervelt, E. R., Grizzle, J. W., Chevallereau, C., Choi, J. H., and Morris, B., 2007, *Feedback Control of Dynamic Bipedal Robot Locomotion*, CRC Press, Boca Raton, FL, p. 528.

[4] Grizzle, J. W., Chevallereau, C., Sinnet, R. W., and Ames, A. D., 2014, "Models, Feedback Control, and Open Problems of 3D Bipedal Robotic Walking," Automatica, **50**(8), pp. 1955–1988.

[5] Sadeghian, H., Ott, C., Garofalo, G., and Cheng, G., 2017, "Passivity-Based Control of Underactuated Biped Robots Within Hybrid Zero Dynamics Approach," IEEE International Conference Robotics and Automation (ICRA), Singapore, May 29–June 3, pp. 4096–4101.

[6] McGeer, T., 1990, "Passive Dynamic Walking," Int. J. Rob. Res., **9**(2), pp. 62–82.

[7] Spong, M. W., and Bhatia, G., 2003, "Further Results on Control of the Compass Gait Biped," IEEE Conference on Intelligent Robots and Systems (IROS), Las Vegas, NV, Oct. 27–31, pp. 1933–1938.

[8] Bloch, A. M., Leonard, N. E., and Marsden, J. E., 2001, "Controlled Lagrangians and the Stabilization of Euler-Poincare Mechanical Systems," Int. J. Robust Nonlinear Control, **11**(3), pp. 191–214.

[9] Holm, J. K., and Spong, M. W., 2008, "Kinetic Energy Shaping for Gait Regulation of Underactuated Bipeds," IEEE International Conference on Control Applications, San Antonio, TX, Sept. 3–5, pp. 1232–1238.

[10] Spong, M. W., and Bullo, F., 2005, "Controlled Symmetries and Passive Walking," IEEE Trans. Autom. Control, **50**(7), pp. 1025–1031.

[11] Gregg, R. D., and Spong, M. W., 2010, "Reduction-Based Control of Three-Dimensional Bipedal Walking Robots," Int. J. Rob. Res., **29**(6), pp. 680–702.

[12] Lv, G., Zhu, H., and Gregg, R. D., 2018, "On the Design and Control of Highly Back Drivable Lower-Limb Exoskeletons: A Discussion of Past and Ongoing Work," IEEE Control Syst. Mag., **38**(6), pp. 88–113.

[13] De-León-Gómez, V., Santibañez, V., and Sandoval, J., 2017, "Interconnection and Damping Assignment Passivity-Based Control for a Compass-Like Biped Robot," Int. J. Adv. Rob. Syst., **14**(4), epub.

[14] Sinnet, R. W., and Ames, A. D., 2015, "Energy Shaping of Hybrid Systems Via Control Lyapunov Functions," American Controls Conference (ACC), Chicago, IL, July 1–3, pp. 5992–5997.

[15] Sinnet, R. W., 2015, "Energy Shaping of Mechanical Systems Via Control Lyapunov Functions With Applications to Bipedal Locomotion," Ph.D. thesis, Texas A&M University, College Station, TX.

[16] Yeatman, M. R., Lv, G., and Gregg, R. D., 2018, "Passivity-Based Control With a Generalized Energy Storage Function for Robust Walking of Biped Robots," American Control Conference (ACC), Milwaukee, WI, June 27–29, pp. 2958–2963.

[17] Wang, S.-H., and Davison, E., 1973, "On the Stabilization of Decentralized Control Systems," IEEE Trans. Autom. Control, **18**(5), pp. 473–478.

[18] Hamed, K. A., and Gregg, R. D., 2017, "Decentralized Feedback Controllers for Robust Stabilization of Periodic Orbits of Hybrid Systems: Application to Bipedal Walking," IEEE Trans. Control Syst. Technol., **25**(4), pp. 1153–1167.

[19] Hamed, K., and Gregg, R. D., 2018, "Decentralized Event-Based Controllers for Robust Stabilization of Hybrid Periodic Orbits: Application to Underactuated 3D Bipedal Walking," IEEE Trans. Autom. Control (epub).

[20] Martin, A. E., and Gregg, R. D., 2017, "Stable, Robust Hybrid Zero Dynamics Control of Powered Lower-Limb Prostheses," IEEE Trans. Autom. Control, **62**(8), pp. 3930–3942.

[21] Lv, G., and Gregg, R. D., 2018, "Underactuated Potential Energy Shaping With Contact Constraints: Application to a Powered Knee-Ankle Orthosis," IEEE Trans. Control Syst. Technol., **26**(1), pp. 181–193.

[22] Ortega, R., Perez, J. A. L., Nicklasson, P. J., and Sira-Ramirez, H., 2013, *Passivity-Based Control of Euler-Lagrange Systems: Mechanical, Electrical and Electromechanical Applications*, Springer Science and Business Media, Berlin.

[23] Murray, R. M., Li, Z., Sastry, S. S., and Sastry, S. S., 1994, *A Mathematical Introduction to Robotic Manipulation*, CRC Press, Boca Raton, FL.

[24] Lv, G., and Gregg, R. D., 2015, "Orthotic Body-Weight Support Through Underactuated Potential Energy Shaping With Contact Constraints," 54th IEEE Conference on Decision and Control (CDC), Osaka, Japan, Dec. 15–18, pp. 1483–1490.

[25] Lv, G., and Gregg, R. D., 2017, "Towards Total Energy Shaping Control of Lower-Limb Exoskeletons," American Control Conference (ACC), Seattle, WA, May 24–26, pp. 4851–4857.

[26] Westervelt, E. R., Grizzle, J. W., and Koditschek, D. E., 2003, "Hybrid Zero Dynamics of Planar Biped Walkers," IEEE Trans. Autom. Control, **48**(1), pp. 42–56.

[27] Sepulchre, R., Jankovic, M., and Kokotovic, P. V., 2012, Constructive Nonlinear Control, Springer Science and Business Media, Berlin.

[28] Spong, M. W., Hutchinson, S., and Vidyasagar, M., 2006, *Robot Modeling and Control*, Vol. 3, Wiley, New York.

[29] Spong, M., Holm, J., and Lee, D., 2007, "Passivity-Based Control of Bipedal Locomotion," IEEE Rob. Autom. Mag., **14**(2), pp. 30–40.

[30] Block, D. J., Åström, K. J., and Spong, M. W., 2007, "The Reaction Wheel Pendulum," Synth. Lect. Control Mechatronics, **1**(1), pp. 1–105.

[31] Zefran, M., Bullo, F., and Stein, M., 2001, "A Notion of Passivity for Hybrid Systems," 40th IEEE Conference on Decision and Control (CDC), Orlando, FL, Dec. 4–7, pp. 768–773.

[32] Naldi, R., and Sanfelice, R. G., 2013, "Passivity-Based Control for Hybrid Systems With Applications to Mechanical Systems Exhibiting Impacts," Automatica, **49**(5), pp. 1104–1116.

[33] Asano, F., Luo, Z.-W., and Yamakita, M., 2005, "Biped Gait Generation and Control Based on a Unified Property of Passive Dynamic Walking," IEEE Trans. Rob., **21**(4), pp. 754–762.

[34] Cheng, M.-Y., and Lin, C.-S., 1996, "Measurement of Robustness for Biped Locomotion Using a Linearized Poincaré Map," Robotica, **14**(3), pp. 253–259.

[35] Koolen, T., De Boer, T., Rebula, J., Goswami, A., and Pratt, J., 2012, "Capturability-Based Analysis and Control of Legged Locomotion—Part 1: Theory and Application to Three Simple Gait Models," Int. J. Rob. Res., **31**(9), pp. 1094–1113.

[36] Hobbelen, D. G., and Wisse, M., 2007, "A Disturbance Rejection Measure for Limit Cycle Walkers: The Gait Sensitivity Norm," IEEE Trans. Robotics, **23**(6), pp. 1213–1224.

[37] Wisse, M., Hobbelen, D. G., Rotteveel, R. J., Anderson, S. O., and Zeglin, G. J., 2006, "Ankle Springs Instead of Arc-Shaped Feet for Passive Dynamic Walkers," Sixth IEEE-RAS International Conference on Humanoid Robots, IEEE, Genova, Italy, Dec. 4–6, pp. 110–116.

[38] Thangal, S. N. M., Talaty, M., and Balasubramanian, S., 2013, "Assessment of Gait Sensitivity Norm as a Predictor of Risk of Falling During Walking in a Neuromusculoskeletal model," Med. Eng. Phys., **35**(10), pp. 1483–1489.

[39] Hobbelen, D. G., and Wisse, M., 2008, "Swing-Leg Retraction for Limit Cycle Walkers Improves Disturbance Rejection," IEEE Trans. Rob., **24**(2), pp. 377–389.

[40] Bhatia, G. S., 2002, "Passivity Based Control of Biped Robots," Master's thesis, University of Illinois, Champaign, IL.

[41] Gordon, D., Robertson, E., and Winter, D. A., 1980, "Mechanical Energy Generation, Absorption and Transfer Amongst Segments During Walking," J. Biomech., **13**(10), pp. 845–854.

[42] Nuño, E., Basañez, L., and Ortega, R., 2011, "Passivity-Based Control for Bilateral Teleoperation: A Tutorial," Automatica, **47**(3), pp. 485–495.